ACS OMEGA

http://pubs.acs.org/journal/acsodf

Article

Highly Stable White Light Emission from III-Nitride Nanowire LEDs Utilizing Nanostructured Alumina-Doped Mn^{4+} and Mg^{2+}

Thi Tuyet Doan, Thanh Quang Le, Boi An Tran, Tung Cao-Thanh Pham, Ravi Teja Velpula, Mano Bala Sankar Muthu, Hieu Pham Trung Nguyen, Quan Thi Hong Vu, Przemysław Jacek Dereń, and Hoang-Duy Nguyen*

Cite This: *ACS Omega* 2023, 8, 2501−2507

Read Online

ACCESS | Metrics & More | Article Recommendations

ABSTRACT: In this report, red-emitting alumina nanophosphors doped with Mn^{4+} and Mg^{2+} (Al_2O_3:Mn^{4+}, Mg^{2+}) are synthesized by a hydrothermal method using a Pluronic surfactant. The prepared samples are ceramic-sintered at various temperatures. X-ray diffraction shows that Al_2O_3:Mn^{4+}, Mg^{2+} annealed at 500 °C exhibits a cubic γ-Al_2O_3 phase with the space group *Fd*3*m*-227. The tetragonal δ-Al_2O_3 and rhombohedral α-Al_2O_3 phase is obtained at 1000 and 1300 °C, respectively. Cube-like nanoparticles in a size of ∼40 nm are observed for the alumina heated at 500−1000 °C. The size and red-emitting intensity of the phosphors remarkably increased with annealed temperature ∼1300 °C. Emission spectra of the phosphors show strong peaks at 678 and 692 nm due to $^2E_g \rightarrow {}^4A_2$ transitions of the Mn^{4+} ion, under a light excitation of 460 nm. A strong zero-phonon line (ZPL) emission is observed in the luminescence spectra of δ-Al_2O_3:Mn^{4+}, Mg^{2+} at 298 K, whereas a weak one is observed in those of α- and γ-Al_2O_3:Mn^{4+}, Mg^{2+}. The alumina phosphors exhibited an excellent waterproof ability during 60 days in water and good thermal stability in the range of 77−573 K. A warm-white light-emitting diode (WLED) fabricated using $In_xGa_{1-x}N$ nanowire chips with Al_2O_3:Mn^{4+}, Mg^{2+} red-emitting nanophosphors presents a high color rendering index of ∼95.1 and a low correlated color temperature of ∼4998 K. Moreover, the current−voltage characteristic of the nanowire LEDs could be improved using Al_2O_3:Mn^{4+}, Mg^{2+} nanophosphors which is attributed to the increased heat dissipation in the nanowire LEDs.

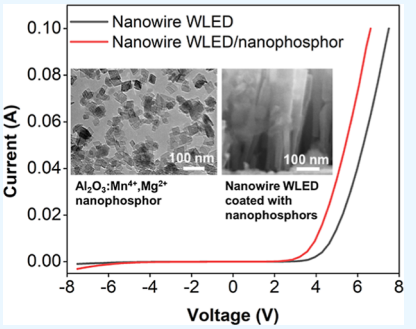

1. INTRODUCTION

Nanostructured III-nitride materials have attracted significant attention due to their great potential applications in micro-displays, conformable light sources, and augment/virtual reality technology. The light-emitting diodes (LEDs) that could emit different wavelengths from ultraviolet (UV), visible light, and infrared (IR) by controlling the In, Ga, and Al composition in In(Al)GaN materials are intensively investigated.[1−8] However, the fabrication of high-efficiency full-color LEDs, especially at long wavelengths (green and red light), remains a challenge that hinders the commercial availability of micro-displays.[8−13] In addition, luminous efficacy of the LEDs can attain 50 to 70% of the theoretical maximum.[14] More than 30% of the energy is converted into heat which reduces the LED luminescent efficacy and lifetime. Recently, high-color rendering index (CRI) micro-white LEDs have been fabricated including blue-emitting InGaN-nanowire devices and red-emitting fluoride nanophosphors.[15,16] Although fluoride phosphors exhibit intensive red emission and easy preparation, they are unstable with high humidity and low thermal conductivity.[17,18] Recently, aluminum oxides such as α-Al_2O_3:Mn^{4+}, Mg^{2+}; $BaMgAl_{10}O_{17}$:Mn^{4+}, Mg^{2+}; $BeAl_2O_4$:Mn^{4+}; $Y_3Al_5O_{12}$:Mn^{4+}, Mg^{2+}; $Lu_3Al_5O_{12}$:Mn^{4+}, Mg^{2+}; and $CaGdAlO_4$:Mn^{4+}, Mg^{2+} (Mg^{2+} as charge compensation ions), prepared via a solid-state reaction at high temperature 1200−1750 °C, have been intensively studied for improving the color reproduction of thin-film white LEDs due to their high red emission intensity, hardness, and good thermal stability.[19−25] The crystal-phase transitions with temperatures of the alumina material have been reported.[26] However, only few studies reported the luminescence properties of Mn^{4+} doped into different Al_2O_3 nanocrystal phases. In this work, we have prepared Al_2O_3:Mn^{4+}, Mg^{2+} (ALO) nanosheets via a hydrothermal route. Calcined ALO pristine at 500−1300 °C exhibited high red emission, low thermal quenching, and excellent water resistance. Furthermore, nanocrystal phases such as α-, δ-, and γ-ALO are obtained at various heating temperatures. A strong zero-phonon line (ZPL) emission is observed in the δ-ALO photoluminescence spectrum. A warm-

Received: October 30, 2022
Accepted: December 22, 2022
Published: January 6, 2023

white LED (WLED) with a high color rendering index (R_a = 95.1) and a low correlated color temperature (CCT) (~4998 K) is fabricated using the ALO nanophosphors and a nanowire−InGaN-based LED emitting blue and yellow light. Additionally, highly stable white light emission has also been demonstrated from these WLEDs. The WLED exhibits significantly improved current−voltage characteristics which is attributed to the increased heat dissipation with the employment of Al_2O_3:Mn^{4+}, Mg^{2+} nanophosphors.

2. RESULTS AND DISCUSSION

2.1. Structural and Morphology Characterizations. X-ray diffraction (XRD) patterns of Al_2O_3:Mn^{4+}, Mg^{2+} calcined at different temperatures are shown in Figure 1a. All the

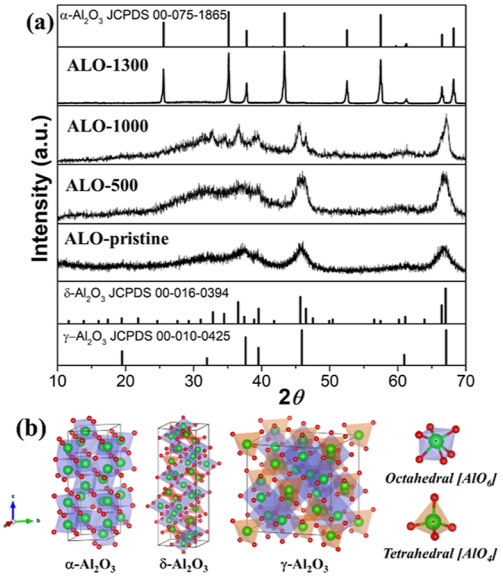

Figure 1. (a) XRD patterns of ALO pristine, ALO-500, ALO-1000, and ALO-1300. (b) Crystal structure of α-Al_2O_3, δ-Al_2O_3, and γ-Al_2O_3 with different coordination environments for Al^{3+} ions as AlO_4 and AlO_6.

diffraction peaks of the ALO pristine and ALO-500 samples can be indexed to cubic γ-Al_2O_3 with space group *Fd*3*m*-227 (JCPDS no. 00-010-0425). The XRD pattern of the ALO-1000 sample shows diffraction peaks matching the standard data (JCPDS no. 00-016-0394) of tetragonal δ-Al_2O_3 with space group I-. The diffraction peaks in the XRD pattern of ALO-1300 corresponded to those of rhombohedral α-Al_2O_3 with space group *R*-3*c*-167 (JCPDS no. 00-075-1865). The sharpened diffracted peaks with high intensity indicate the enhanced crystallinity of nanoparticles at 1300 °C.

The crystal structures of α-Al_2O_3, δ-Al_2O_3, and γ-Al_2O_3 are presented in Figure 1b. In the γ-Al_2O_3 structure, the oxygen atoms are arranged in a cubic lattice, while the Al^{3+} ions occupy the tetrahedral (Al^{3+} with fourfold coordination by O^{2-}, AlO_4) and octahedral (Al^{3+} with sixfold coordination by O^{2-}, AlO_6) interstitial sites of the lattice. The α-Al_2O_3 structure consists of a hexagonal close-packed array of oxygen atoms with the Al atoms occupying the octahedral interstices. δ-Al_2O_3 has been considered a spinel structure with tetragonal distortions. The structures adopt a complex crystallography and disorder with freedom arrangement of Al^{3+} in tetrahedral and octahedral sites.[27] It is known that occupancy and stability of Mn^{4+} ions are observed in AlO_6 sites.[28−30]

Field-emission scanning electron microscopy (FESEM) images of Al_2O_3:Mn^{4+}, Mg^{2+} samples are presented in Figure 2a−d. The FESEM images of ALO pristine, ALO-500, and

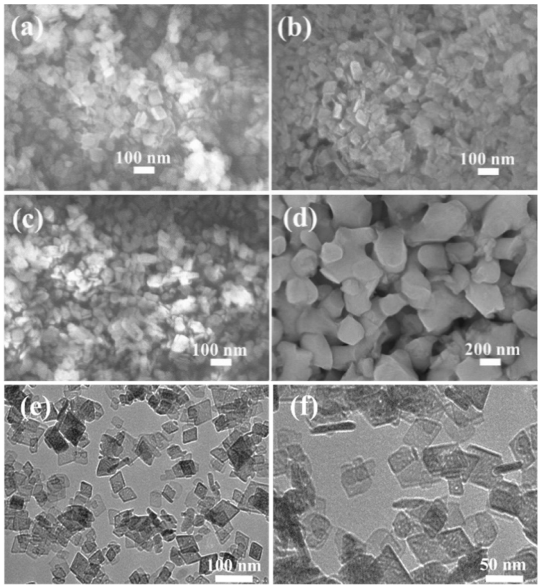

Figure 2. FESEM images of (a) ALO pristine, (b) ALO-500, (c) ALO-1000, and (d) ALO-1300. (e,f) TEM images of ALO-500 at different magnifications.

ALO-1000 show cube-like ALO nanoparticles. Transmission electron microscopy (TEM) images of ALO-500 present the nanosheets with an average size of ~40 nm and a thickness of 5 nm (Figure 2e,f). When the samples were calcined at high temperatures up to ~1300 °C, the particle size remarkably increased to ~200−400 nm (Figure 2d).

The surface and cross-section FESEM images of the nanowire-InGaN wafer coated with ALO-500 are shown in Figure 3a,b, respectively. The average diameter, length, and adjacent distance of nanowires are estimated to be ~90, 500, and 55 nm, respectively. The distribution of ALO-500 nanosheets in between the nanowires is obviously observed as shown in the inset of Figure 3b. The SEM image of the nanowire LED coated with ALO-1300 is shown in Figure 3c.

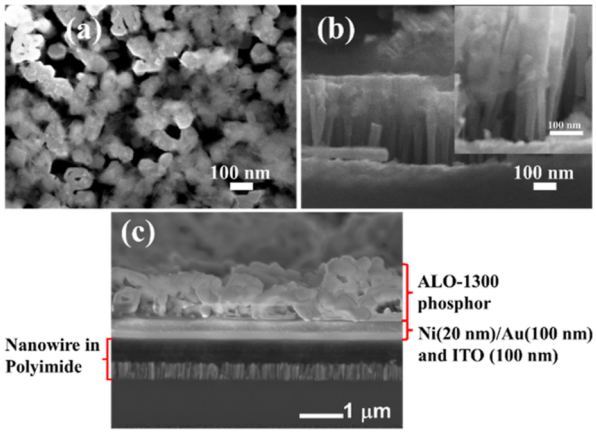

Figure 3. FESEM images of (a) surface and (b) cross-section of nanowire LEDs coated with ALO-500. The inset picture presents the high-magnification image of the nanowires. (c) SEM image of the nanowire LED with ALO-1300 on the top electrode.

https://doi.org/10.1021/acsomega.2c06990
ACS Omega 2023, 8, 2501−2507

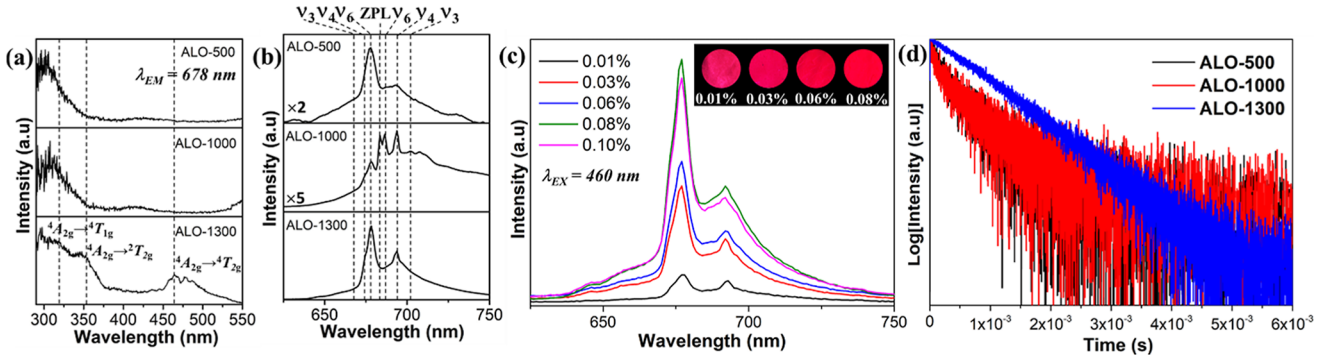

Figure 4. (a) PLE and (b) PL spectra of ALO-500, ALO-1000, and ALO-1300 at 298 K. (c) PL spectra of ALO-1300 at different Mn^{4+} amounts. The inset picture shows the emission of ALO-1300 at various Mn^{4+} concentrations under 365 nm light excitation. (d) PL decay curves of ALO-500, ALO-1000, and ALO-1300 at 289 K.

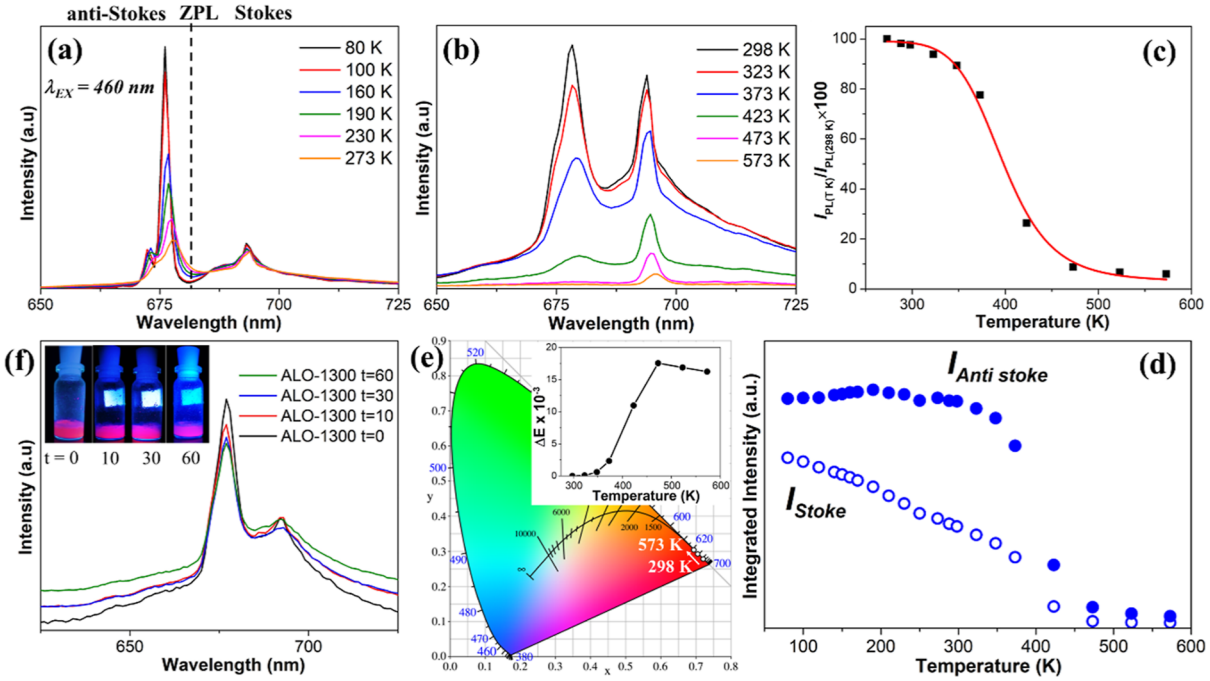

Figure 5. Temperature-dependent emission spectra of ALO-1300 in a temperature range of (a) 80−273 K and (b) 298−573 K. (c) Relative red PL intensity as a function of temperature (273−573 K). The solid line represents the fitting result with the expression $I_T/I_0 = [1 + D\exp(-E_a/kT)]^{-1}$ in 273−573 K. (d) Integrated intensity of anti-Stokes and Stokes emission lines. (e) CIE chromaticity coordinates (x,y) of ALO-1300 with temperatures. The inset picture shows the chromaticity (x,y) shift from 298 to 573 K of ALO-1300. (f) PL spectra of ALO-1300 in deionized water at various times. The inset picture shows the emission of ALO-1300 in water at different durations under 365 nm light excitation.

The top electrode including Ni(20 nm)/Au(100 nm) and indium tin oxide(100 nm), nanowires in polyimide, and the ALO-1300 phosphor layer are clearly presented. The thickness of the ALO-1300 phosphor on the LED is estimated to be ∼1.15 μm.

2.2. Photoluminescence Properties. The photoluminescence excitation (PLE) and PL spectra of the $Al_{2-2x}O_3:Mn_x^{4+}$, Mg_x^{2+} (x = 0.08%) samples were recorded at room temperature (Figure 4). The excitation bands of the ALO-1300 sample are located at the 300−500 nm region with the maxima at 316 nm and 474 nm attributed to the $^4A_{2g} \rightarrow {}^4T_{1g}$ and $^4A_{2g} \rightarrow {}^4T_{2g}$ spin-allowed transitions of Mn^{4+}, respectively, and a weak peak at 356 nm assigned to the $^4A_{2g} \rightarrow {}^2T_{2g}$ spin-forbidden transition of Mn^{4+} (Figure 4a). For ALO-500 and ALO-1000 nanophosphors, these peaks have a blue shift at 308 nm ($^4A_{2g} \rightarrow {}^4T_{1g}$), 420 nm ($^4A_{2g} \rightarrow {}^4T_{2g}$), and 325 nm ($^4A_{2g} \rightarrow {}^2T_{2g}$). The emission at 678 nm (λ_{em} = 678 nm) was monitored. Figure 4b depicts the PL of the Mn^{4+}-doped alumina nanophosphors on excitation of 460 nm. The PL spectra of ALO-500, ALO-1000, and ALO-1300 exhibited a red emission band in 650−725 nm, which is originated from $^2E_g \rightarrow {}^4A_{2g}$ spin-forbidden transitions of the Mn^{4+} ion. The emission intensity remarkably increased for samples calcined at a high temperature of 1300 °C because of their better crystallinity. The emission spectra under 460 nm light excitation presented seven narrow lines at 667, 672, 678, 683, 686, 693, and 702 nm due to transitions of the $\nu_3(t_{1u})$, ν_4 (t_{1u}), ν_6 (t_{2u}), ZPL, ν_6 (t_{2u}), ν_4 (t_{1u}), and $\nu_3(t_{1u})$ vibronic modes, respectively. The ZPL emission intensity at 683 nm, depending on the local symmetry of the Mn^{4+} ion surroundings, was extremely low in α-Al_2O_3 and γ-Al_2O_3 but high in δ-Al_2O_3. The emission spectra of the $Al_{2-2x}O_3:Mn_x^{4+}$, Mg_x^{2+} samples at different Mn^{4+} amounts (∼0.01, 0.03, 0.06, 0.08, and 0.1% mol) are presented in Figure 4c. Under a light

https://doi.org/10.1021/acsomega.2c06990
ACS Omega 2023, 8, 2501−2507

excitation of 460 nm, the emission intensity of ALO-1300 initially increased with an increase in the doping concentration, reached its maximum value when the Mn^{4+} concentration was 0.08% mol, and then decreased upon further increase in the doping concentration because of concentration quenching. The inset shows the dependence of the red emission intensity of ALO-1300 on the Mn^{4+} ion concentration, under 365 nm light excitation. A quantum yield of ∼9.6 and 31.6% was obtained for ALO-500 and ALO-1300 (with the Mn ion doping content ∼0.08% for both samples), respectively, under a 460 nm light excitation. The room temperature (RT) luminescent decay characteristics of the emitting state ^2E_g in the ALO-500, ALO-1000, and ALO-1300 ($[Mn^{4+}] = [Mg^{2+}]$ = 0.08% mol) nanoparticles are shown in Figure 4d. The ALO-1300 sample exhibited a single exponential decay, while the ALO-500 and ALO-1000 samples were fitted well to the non-exponential function. The emission lifetime of ALO-500 (γ-Al_2O_3) is estimated to be 496.2 μs. For the ALO-1000 (δ-Al_2O_3) and ALO-1300 (α-Al_2O_3) samples, the decay times are ∼654.2 and 908.4 μs, respectively. The emission decay of ALO-1300 is longer than that of ALO-1000 and ALO-500. It might be due to increase in native defects in Al_2O_3 crystal-phase transition with the rising annealing temperature. The excited electron may be trapped into the intrinsic defects.[15,20]

The temperature-dependent emission spectra of ALO-1300 under 460 nm light excitation are presented in Figure 5a,b. When the temperature was increased from 80 to 573 K, all the emission lines became broader and red-shifted because of the increase in photon absorption and the enhanced vibration transition coupling associated with the vibration modes of the MnO_6 octahedron.[25,31] The temperature-dependent behavior of the integrated PL intensity $[I_{PL(TK)}/I_{PL(273K)}]$ demonstrated considerable stability for the nanophosphor within the temperature range of 273−573 K (Figure 5c). At 373 K, the relative PL intensity of the sample remained 77.5% at 273 K. It indicated good thermal stability of prepared alumina nanophosphors. Non-radiative transition probability increased with temperature, and integrated PL intensity exhibited thermal quenching, which can be fitted by $I_T/I_0 = [1 + D\exp(-E_a/kT)]^{-1}$, where I_0 is the initial emission intensity, I_T is the intensity at temperature T, E_a is the activation energy, D is a constant, and k is the Boltzmann's constant. The thermal activation energies obtained for ALO-1300 are ∼0.66 ± 0.04 eV. Figure 5d shows that the integrated intensity of anti-Stokes emission lines slightly increased in the temperature range of 80−298 K whereas that of Stokes emission gradually decreased, and then, both degraded with further increasing temperature. Figure 5e displays the variation in the International Commission on Illumination (CIE) chromaticity coordinates of ALO-1300 at different temperatures. At 298 K, the CIE coordinates of ALO-1300 were (0.7216, 0.2784), showing a deep-red emission compared to that of the currently reported K_2SiF_6:Mn^{4+} nanophosphors with chromaticity coordinate (0.7102, 0.2870).[16] The calculated CIE shifts of ALO-1300 within the temperature range of 298−573 K are calculated by following eq 1 and plotted in the inset picture of Figure 5e. The chromaticity shifts (ΔE) were 2.3×10^{-3} at 373 K and 16.2×10^{-3} at 573 K, which indicates the excellent chromaticity stability of the prepared alumina nanophosphors. The moisture resistance of the ALO-1300 sample was tested by measuring its emission in deionized water at different durations, including t = 0, 10, 30, and 60 days, under the 460 nm light excitation. The emission intensity of ALO-1300 unremarkably decreased after immersing in water, as displayed in Figure 5f. The integrated luminescence intensity values ($I_{PL\ at\ t}/I_{PL\ at\ t=0}$) of the sample were 89.0%, 83.9, and 80.9% at 10, 30, and 60 days, respectively, which indicated super waterproof ability of prepared Al_2O_3:Mn^{4+}, Mg^{2+}.

$$\Delta E = \sqrt{(u_t' - u_0')^2 + (v_t' - v_0')^2 + (w_t' - w_0')^2} \quad (1)$$

where $u' = 4x/(3 - 2x + 12y)$, $v' = 9y/(3 - 2x + 12y)$, and $w' = 1 - u' - v'$ are the chromaticity coordinates in uniform color space 1976 and x and y are the chromaticity coordinates in CIE 1931. The 0 and t subscripts denote room-temperature and high-temperature parameters, respectively.

2.3. Electroluminescence Properties. Figure 6a,b presents the electroluminescence (EL) spectra of the reference

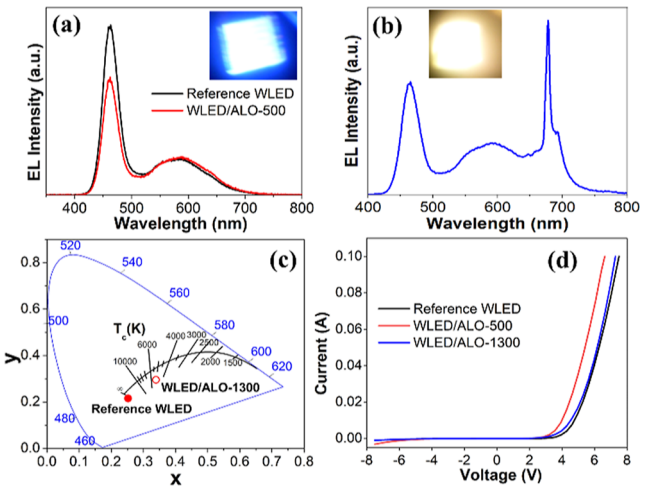

Figure 6. Electroluminescence spectra of (a) reference WLED and the WLED coated with ALO-500 and (b) WLED coated with ALO-1300, measured at room temperature. Inset pictures show bright white light emitted from the fabricated WLEDs. (c) CIE chromaticity coordinate of the WLED coated with ALO-1300. (d) I−V characteristics of the reference WLED, the WLED coated with ALO-500, and the WLED coated with ALO-1300.

WLED, the WLED coated with ALO-500, and the WLED coated with ALO-1300. As shown in Figure 6a, the reference WLED exhibits strong emissions at 461 and 590 nm, while the dominant peak emission at 461 nm can be used as an excitation source for the ALO-1300 nanophosphors. The inset shows the optical cool-white emission from this WLED. The WLED coated with ALO-500 only shows two peaks which are at 461 and 590 nm and are similar to those of the reference WLED due to the weak emission (678 nm) from ALO-500. As illustrated in Figure 6b, the WLED coated with ALO-1300 has an additional peak emission at 678 nm which is related to the emission from ALO-1300 nanophosphors. The intensity of the blue emission in this WLED is reduced compared to that in the reference WLED due to the strong absorption by ALO-1300. The WLED with ALO-1300 shows a strong emission with a high CRI of 95.1. The inset shows the optical emission of this WLED under 100 mA injection current. The CIE diagram, presented in Figure 6c, shows a white emission from the WLED coated with ALO-1300 with the x and y values being 0.3391 and 0.2953, respectively. Due to the contribution of red emission from the ALO, the corresponding CCT of this WLED is measured to be 4998 K which is significantly lower than that of the reference WLED recorded at 57953 K. The

https://doi.org/10.1021/acsomega.2c06990
ACS Omega 2023, 8, 2501−2507

electrical properties of the WLEDs were characterized using Keithley 2401, as presented in Figure 6d. The WLEDs exhibit excellent current−voltage characteristics with low leakage current which is about a few micro-amps at −7 V. At 20 mA, the corresponding voltages of the reference WLED, the WLED with ALO-1300, and the WLED with ALO-500 are 5.29, 5.11, and 4.42 V, respectively. However, compared to the reference WLED, the WLED coated with ALO-1300 shows better current−voltage properties with lower series resistance which is attributed to the reduced heating effect or the increased heat dissipation by using ALO-1300 on the top surface of the WLED. The WLED coated with ALO-500 shows the best current−voltage properties with significantly reduced resistance compared to the reference WLED and WLED with ALO-1300. This can be attributed to the more efficient heat dissipation via ALO-500 (∼40 nm in size) in between the nanowires compared to that of applying ALO-1300 (∼300 nm in size) only on the top surface of the LEDs.[32−34]

As presented in Figure 7a, the WLED coated with ALO-1300 exhibits highly stable white light emissions under

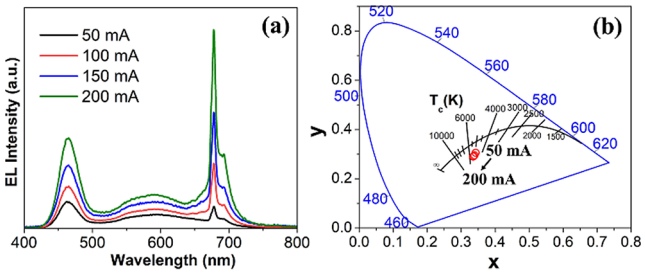

Figure 7. (a) EL spectra of the WLED coated with ALO-1300 measured at different injection currents. (b) CIE chromaticity coordinate of the WLED coated with ALO-1300 under injection current from 50 to 200 mA.

injection current from 50 to 200 mA. An invisible shift was observed for the peak emissions at 461, 590, and 678 nm attributed to the negligible quantum-confined Stark effect and reduced heating effect in this high-crystalline quality nanowire LED structure and the utilization of ALO.[13,27,30] The EL spectra of this WLED do not show significant variation with increasing injection currents, resulting in highly stable emission characteristics, as shown in Figure 7b. It is seen that the WLED coated with ALO-1300 has stable CIE chromaticity coordinates with the x and y values in the ranges of 0.3391−0.354 and 0.2953−0.2899, respectively.

3. CONCLUSIONS

In conclusion, Al_2O_3:Mn^{4+}, Mg^{2+} cube-like nanoparticles are synthesized via a hydrothermal method. The cubic γ-Al_2O_3, tetragonal δ-Al_2O_3, and rhombohedral α-Al_2O_3 phases are obtained by annealing the pristine nanoparticles at 500 °C, at 1000, and at 1300 °C, respectively. The prepared samples possess a deep-red emission under 460 nm light excitation. The ZPL emission intensity at 683 nm is extremely low in the luminescence spectra of α- and γ-Al_2O_3:Mn^{4+}, Mg^{2+} but significantly high in those of δ-Al_2O_3:Mn^{4+}, Mg^{2+}; this indicates the different crystal symmetry of the Mn^{4+} ion surroundings. The luminescence intensity of ALO-1300 submicron particles (200−400 nm) remarkably increases with quantum yield ∼31.6% compared to that of ALO-500 nanoparticles (40 nm) ∼9.1%. Importantly, the nanophosphors exhibited an excellent waterproof ability and low thermal quenching. The WLEDs coated with ALO-1300 show a stable white emission with a high CRI of 95.1 at a CCT of 4998 K. Moreover, the nanowire WLEDs with Al_2O_3:Mn^{4+}, Mg^{2+} nanophosphors exhibit improved current−voltage characteristics which are attributed to the increased heat dissipation in the nanowire LEDs. The present study demonstrates that the ALO nanomaterial is a promising red component for the cost-effective micro-WLEDs, which are highly expected for the next-generation display technology. This study demonstrates a promising approach for improving the color reproducibility of WLEDs that can be suitable for practical applications that may include micro-displays and augmented reality/virtual reality devices.

4. EXPERIMENTAL SECTION

4.1. Nanophosphor $Al_{2-2x}O_3$:Mn_x^{4+}, Mg_x^{2+} Synthetic Procedures. All chemicals were of standard grade and used as received without further purification. Nanosized $Al_{2-2x}O_3$:Mn_x^{4+}, Mg_x^{2+} (x = 0.01−0.1%) phosphors were synthesized through a hydrothermal route. 500 μL of 1.2 × 10^{-3}−12 × 10^{-3} M $MgSO_4$ and $MnSO_4$ solution was added into a mixture of 4.5 g of $Al(NO_3)_3{\cdot}9H_2O$ and 0.045 g of a Pluronic F68 surfactant dissolved into 50 mL of deionized water. The solution pH was adjusted to ∼9.5 by dropping 10% NH_4OH solution and stirring for 2 h. The suspension was transferred into a 100 mL Teflon-lined stainless-steel autoclave, and the hydrothermal process was carried out at 200 °C for 24 h. The obtained white powder was rinsed with deionized water until pH ∼7 and then with the acetone solvent. The powder was dried at 50 °C in an oven. Lastly, ALO-pristine nanoparticles were heated at 300 °C for 30 min and annealed at 500 °C (ALO-500) or 1000 °C (ALO-1000) or 1300 °C (ALO-1300) for 3 h.

4.2. Structural and Optical Characterizations. The purity and structure of the samples were examined via XRD on a Bruker AXS D8 ADVANCE ECO diffractometer equipped with a LYNXEYE XE-T detector and Cu Kα radiation (λ = 1.54059 Å). A field-enhanced scanning electron microscope (Hitachi FESEM S4800, Japan) and transmission electron microscope (JEOL, JSM-1400) were used to characterize the morphology of the materials. A McPherson spectrometer with a 150 W xenon lamp and a Hamamatsu R928 photomultiplier (Hamamatsu Photonics K. K, Shizuoka, Japan) was used to measure the RT excitation spectra. Luminescence spectra and temperature-dependent luminescence of the samples were studied with a Hamamatsu photonic multichannel analyzer PMA-12 equipped with a BT-CCD linear image sensor (Hamamatsu Photonics KK, Shizuoka, Japan). The temperature of the samples was controlled using a Linkam THMS 600 Heating/Freezing Stage (The McCrone Group, Westmont, IL, USA). The quantum yield was measured using a Hamamatsu PMA-12 spectrophotometer equipped with an integrating sphere. Decay profiles of all samples were measured by using a Tektronix MD3052 mixed domain oscilloscope 500 MHz (Beaverton, OR, US) and a Nd:YAG laser (Teledyne LeCroy, New York, NY, USA).

4.3. InGaN Nanowire Phosphor-Converted (pc) WLED Fabrication. The InGaN/AlGaN core−shell nanowire LED heterostructures on a Si substrate were grown using a Veeco Gen II molecular beam epitaxy (MBE) system. The Si substrate was processed by standard cleaning procedures that include cleaning with isopropanol, acetone, deionized water,

https://doi.org/10.1021/acsomega.2c06990
ACS Omega 2023, 8, 2501−2507

and then hydrofluoric acid (10%) solution. The substrate was then loaded into the MBE chambers for subsequent thermal cleaning processes at 550 and 800 °C for 2 h and 15 min, respectively. The epitaxial growth of the nanowire structure was initiated with a ∼200 nm GaN/Si nanowire segment, followed by the device active region consisting of 10 InGaN/AlGaN quantum wells. Each quantum well includes a 3 nm InGaN well and 3 nm AlGaN barrier. Finally, ∼200 nm GaN/Mg was grown on the top of the active region to finish the epitaxial growth experiment. During the growth process, the nitrogen flow rate was kept at 1.0 standard cubic centimeter per minute (sccm), with a forward plasma power of ∼350 W. The GaN/Si and GaN/Mg segments were grown at ∼800 °C. During the growth of the InGaN/AlGaN active region, the substrate temperature was reduced to 650−680 °C to enhance In incorporation in the dots. After being grown by MBE, the nanowire LED samples were fabricated using standard fabrication processes. The detailed descriptions of the MBE growth and device fabrication of our nanowire LEDs can be found in our previous publications.[8−14]

The fabricated nanowire LEDs with an area size of 300 × 300 μm^2 were selected for the experiment with ALO-1300 (∼300 nm in size). WLEDs were fabricated by coating an isopropanol solution of 10% nanophosphors onto the nanowire-InGaN LED surface via an MS-B100 spin coater. To compare the effectiveness of the alumina nanophosphors, we have applied the ALO-500 nanophosphor (∼40 nm in size) in the gap between nanowires and compared the current−voltage of these LEDs to that of others. The electroluminescence emission of the LED devices was collected using an optical fiber and analyzed using a USB2000 Ocean Optics spectrometer. The measurement was performed under the CW injection current condition.

AUTHOR INFORMATION

Corresponding Author

Hoang-Duy Nguyen − *Institute of Chemical Technology, Vietnam Academy of Science and Technology, Ho Chi Minh City 700000, Vietnam;* orcid.org/0000-0003-2002-8417; Email: nhduy@iams.vast.vn

Authors

Thi Tuyet Doan − *Institute of Chemical Technology, Vietnam Academy of Science and Technology, Ho Chi Minh City 700000, Vietnam*

Thanh Quang Le − *Institute of Chemical Technology, Vietnam Academy of Science and Technology, Ho Chi Minh City 700000, Vietnam*

Boi An Tran − *Institute of Chemical Technology, Vietnam Academy of Science and Technology, Ho Chi Minh City 700000, Vietnam;* orcid.org/0000-0001-7049-0226

Tung Cao-Thanh Pham − *Institute of Chemical Technology, Vietnam Academy of Science and Technology, Ho Chi Minh City 700000, Vietnam;* orcid.org/0000-0002-4631-481X

Ravi Teja Velpula − *Helen and John C. Hartmann Department of Electrical and Computer Engineering, New Jersey Institute of Technology, Newark, New Jersey 07102, United States*

Mano Bala Sankar Muthu − *Helen and John C. Hartmann Department of Electrical and Computer Engineering, New Jersey Institute of Technology, Newark, New Jersey 07102, United States*

Hieu Pham Trung Nguyen − *Helen and John C. Hartmann Department of Electrical and Computer Engineering, New Jersey Institute of Technology, Newark, New Jersey 07102, United States;* orcid.org/0000-0003-1129-9581

Quan Thi Hong Vu − *Institute of Chemical Technology, Vietnam Academy of Science and Technology, Ho Chi Minh City 700000, Vietnam; Optical Spectroscopy Department, W Trzebiatowski Institute of Low Temperature and Structural Research of the Polish Academy of Sciences, Wrocław 50-013, Poland;* orcid.org/0000-0001-9390-3994

Przemysław Jacek Dereń − *Optical Spectroscopy Department, W Trzebiatowski Institute of Low Temperature and Structural Research of the Polish Academy of Sciences, Wrocław 50-013, Poland;* orcid.org/0000-0001-6316-6954

Complete contact information is available at: https://pubs.acs.org/10.1021/acsomega.2c06990

Author Contributions

The manuscript was written through contributions of all authors.

Notes

The authors declare no competing financial interest.

ACKNOWLEDGMENTS

This research is funded by the Vietnam Academy of Science and Technology under grant number VAST07.02/21-22.

REFERENCES

(1) Chen, F.; Ji, X.; Lau, S. P. Recent progress in group III-nitride nanostructures: From materials to applications. *Mater. Sci. Eng. R Rep.* **2020**, *142*, 100578.

(2) Wu, Y.; Liu, X.; Pandey, A.; Zhou, P.; Dong, W. J.; Wang, P.; Min, J.; Deotare, P.; Kira, M.; Kioupakis, E.; Mi, Z. III-nitride nanostructures: Emerging applications for Micro-LEDs, ultraviolet photonics, quantum optoelectronics, and artificial photosynthesis. *Prog. Quant. Electron.* **2022**, *85*, 100401.

(3) Bui, H. Q. T.; Dang, H. A.; Doan, T. T.; Velpula, R. T.; Jain, B.; Nguyen, H. P. T.; Nguyen, H.-D. Enhancing Efficiency of AlGaN Ultraviolet-B Light-Emitting Diodes with Graded p-AlGaN Hole Injection Layer. *Phys. Status Solidi A* **2021**, *218*, 2100003.

(4) Velpula, R. T.; Jain, B.; Patel, M.; Shakiba, F. M.; Toan, N. Q.; Nguyen, H.-D.; Nguyen, H. P. T. High-efficiency InGaN blue LEDs with reduced positive sheet polarization. *Appl. Opt.* **2022**, *61*, 4967−4970.

(5) Nguyen, H. P. T.; Zhang, S.; Cui, K.; Korinek, A.; Botton, G. A.; Mi, Z. High-efficiency InGaN/GaN dot-in-a-wire red light-emitting diodes. *IEEE Photon. Technol. Lett.* **2012**, *24*, 321−323.

(6) Philip, M. R.; Choudhary, D. D.; Djavid, M.; Bhuyian, M. N.; Piao, J.; Pham, T. T.; Misra, D.; Nguyen, H. P. Controlling color emission of InGaN/AlGaN nanowire light-emitting diodes grown by molecular beam epitaxy. *J. Vac. Sci. Technol.* **2017**, *35*, 02B108.

(7) Ajay, A.; Kotsar, Y.; Monroy, E. Infrared emitters using III-nitride semiconductors. In *Nitride Semiconductor Light-Emitting Diodes (LEDs)*; Elsevier, 2018; pp 587−617.

(8) Bui, H. Q. T.; Velpula, V.; Jain, J.; Aref, O. H.; Nguyen, H. D.; Lenka, T. R.; Nguyen, H. P. T. Full-color InGaN/AlGaN nanowire micro light-emitting diodes grown by molecular beam epitaxy: A promising candidate for next generation micro displays. *Micromachines* **2019**, *10*, 492.

(9) Jain, B.; Velpula, R. T.; Bui, H. Q. T.; Nguyen, H.-D.; Lenka, T. R.; Nguyen, T. K.; Nguyen, H. P. T. High performance electron blocking layer-free InGaN/GaN nanowire white-light-emitting diodes. *Opt. Express* **2020**, *28*, 665−675.

(10) Rajan Philip, M.; Choudhary, D. D.; Djavid, M.; Bhuyian, M. N.; Bui, T. H. Q.; Misra, D.; Khreishah, A.; Piao, J.; Nguyen, H. D.; Le, K. Q.; Nguyen, H. P. T. Fabrication of phosphor-free III-nitride nanowire light-emitting diodes on metal substrates for flexible photonics. *ACS Omega* **2017**, *2*, 5708−5714.
(11) Nguyen, H. P.; Cui, K.; Zhang, S.; Djavid, M.; Korinek, A.; Botton, G. A.; Mi, Z. Controlling electron overflow in phosphor-free InGaN/GaN nanowire white light-emitting diodes. *Nano Lett.* **2012**, *12*, 1317−1323.
(12) Nguyen, H. P. T.; Zhang, S.; Connie, A. T.; Kibria, M. G.; Wang, Q.; Shih, I.; Mi, Z. Breaking the carrier injection bottleneck of phosphor-free nanowire white light-emitting diodes. *Nano Lett.* **2013**, *13*, 5437−5442.
(13) Nguyen, H. P.; Zhang, S.; Cui, K.; Han, X.; Fathololoumi, S.; Couillard, M.; Botton, G. A.; Mi, Z. p-Type modulation doped InGaN/GaN dot-in-a-wire white-light-emitting diodes monolithically grown on Si(111). *Nano Lett.* **2011**, *11*, 1919−1924.
(14) Andonova, A.; Kim, N.; Vakrilov, N. Estimation the Amount of Heat Generated by LEDs under Different Operating Conditions. *Elektron. Elektrotech.* **2016**, *22*, 49−53.
(15) Tuyet, D. T.; Hong Quan, V. T.; Bondzior, B.; Dereń, P. J.; Velpula, R. T.; Trung Nguyen, H. P.; Tuyen, L. A.; Hung, N. Q.; Nguyen, H. D. Deep red fluoride dots-in-nanoparticles for high color quality micro white light-emitting diodes. *Opt. Express* **2020**, *28*, 26189−26199.
(16) Vu, T. H. Q.; Doan, T. T.; Jain, B.; Velpula, R. T.; Pham, T. C. T.; Nguyen, H. P. T.; Nguyen, H.-D. Improving Color Quality of Nanowire White Light-Emitting Diodes with Mn^{4+} Doped Fluoride Nanosheets. *Micromachines* **2021**, *12*, 965.
(17) Nguyen, H. D.; Lin, C. C.; Liu, R. S. Waterproof alkyl phosphate coated fluoride phosphors for optoelectronic materials. *Angew. Chem.* **2015**, *54*, 10862−10866.
(18) Verstraete, R.; Sijbom, H. F.; Joos, J. J.; Korthout, K.; Poelman, D.; Detavernier, C.; Smet, P. F. Red Mn^{4+}-doped fluoride phosphors: Why purity matters. *ACS Appl. Mater. Interfaces* **2018**, *10*, 18845−18856.
(19) Tian, C.; Lin, H.; Zhang, D.; Zhang, P.; Hong, R.; Han, Z.; Qian, X.; Zou, J. Mn^{4+} activated Al_2O_3 red-emitting ceramic phosphor with excellent thermal conductivity. *Opt. Express* **2019**, *27*, 32666−32678.
(20) Xu, Y.; Wang, L.; Qu, B.; Li, D.; Lu, J.; Zhou, R. The role of co-dopants on the luminescent properties of α-Al_2O_3:Mn^{4+} and $BaMgAl_{10}O_{17}$:Mn^{4+}. *J. Am. Ceram. Soc.* **2019**, *102*, 2737−2744.
(21) Chen, D.; Zhou, Y.; Xu, W.; Zhong, J.; Ji, Z.; Xiang, W. Enhanced Luminescence of Mn^{4+}:$Y_3Al_5O_{12}$ Red Phosphor via Impurity Doping. *J. Mater. Chem. C* **2016**, *4*, 1704−1712.
(22) Zhang, Y.; Hu, S.; Liu, Y.; Wang, Z.; Ying, W.; Zhou, G.; Wang, S. Preparation, crystal structure and luminescence properties of red-emitting $Lu_3Al_5O_{12}$:Mn^{4+} ceramic phosphor. *J. Eur. Ceram. Soc.* **2019**, *39*, 584−591.
(23) Hu, J.; Huang, T.; Zhang, Y.; Lu, B.; Ye, H.; Chen, B.; Xia, H.; Ji, C. Enhanced deep-red emission from Mn^{4+}/Mg^{2+}codoped $CaGdAlO_4$ phosphors for plant cultivation. *Dalton Trans.* **2019**, *48*, 2455−2466.
(24) Hu, J.; Zhao, Y.; Chen, B.; Xia, H.; Zhang, Y.; Ye, H. An investigation of Mn^{4+} doped $BeAl_2O_4$ single crystal for WLEDs Application. *Ceram. Int.* **2018**, *44*, 20220−20226.
(25) Adachi, S. Mn^{4+}-activated red and deep red-emitting phosphors. *ECS J. Solid State Sci. Technol.* **2019**, *9*, 016001.
(26) Mahat, A. M.; Mastuli, M. S.; Kamarulzaman, N. Influence of annealing temperature on the phase transformation of Al_2O_3. *AIP Conference Proceedings*; AIP Publishing LLC, 2016; p 050001.
(27) Kovarik, L.; Bowden, M.; Szanyi, J. High temperature transition aluminas in δ-Al_2O_3/θ-Al_2O_3 stability range. *J. Catal.* **2021**, *393*, 357−368.
(28) Wu, Y.; Zhuang, Y.; Xie, R.-J.; Ruan, K.; Ouyang, X. Novel Mn^{4+} doped red phosphors composed of $MgAl_2O_4$ and $CaAl_{12}O_{19}$ phases for light-emitting diodes. *Dalton Trans.* **2020**, *49*, 3606−3614.
(29) Luo, L.; Liu, R.; Liu, Y.; Zhuang, W.; Li, Y.; Qin, S. Enhanced luminescence performances of Mn^{4+}-activated $Sr_4Al_{14}O_{25}$ red phosphors by doping with Sc^{3+} ions. *J. Rare Earths* **2021**, *39*, 380−385.
(30) Cao, R.; Ye, Y.; Peng, Q.; Chen, T.; Ao, H.; Xiao, F.; Luo, Z.; Liu, P. Deep-Red-Emitting $Na_{1.57}Zn_{0.57}Al_{10.43}O_{17}$: Mn^{4+} Phosphor: Synthesis and Photoluminescence Properties. *J. Electron. Mater.* **2018**, *47*, 7537−7543.
(31) Dhoble, S. J.; Priya, R.; Dhoble, N.; Pandey, O. Short review on recent progress in Mn^{4+}-activated oxide phosphors for indoor plant light-emitting diodes. *Luminescence* **2021**, *36*, 560−575.
(32) Yacobi, B.; Holt, D. Cathodoluminescence scanning electron microscopy of semiconductors. *J. Appl. Phys.* **1986**, *59*, R1−R24.
(33) Vilà, A.; Hernández-Ramirez, F.; Rodríguez, J.; Casals, O.; Romano-Rodríguez, A.; Morante, J.; Abid, M. Fabrication of metallic contacts to nanometre-sized materials using a focused ion beam (FIB). *Mater. Sci. Eng., C* **2006**, *26*, 1063−1066.
(34) Gong, Z.; Jin, S.; Chen, Y.; McKendry, J.; Massoubre, D.; Watson, I. M.; Gu, E.; Dawson, M. D. Size-dependent light output, spectral shift, and self-heating of 400 nm InGaN light-emitting diodes. *J. Appl. Phys.* **2010**, *107*, 013103.

https://doi.org/10.1021/acsomega.2c06990
ACS Omega 2023, 8, 2501−2507